A&A 366, 407–417 (2001)
DOI: 10.1051/0004-6361:20000105

Astronomy & Astrophysics

Testing current synthesis models of the X–ray background

R. Gilli[1,2], M. Salvati[3], and G. Hasinger[2]

[1] Dipartimento di Astronomia e Scienza dello Spazio, Università di Firenze, Largo E. Fermi 5, 50125 Firenze, Italy
e-mail: gilli@arcetri.astro.it
[2] Astrophysikalisches Institut Potsdam, An der Sternwarte 16, 14482 Potsdam, Germany
e-mail: ghasinger@aip.de
[3] Osservatorio Astrofisico di Arcetri, Largo E. Fermi 5, 50125 Firenze, Italy
e-mail: salvati@arcetri.astro.it

Received 3 October 2000 / Accepted 14 November 2000

Abstract. We present synthesis models of the X–ray background where the available X–ray observational constraints are used to derive information on the AGN population properties. We show the need for luminous X–ray absorbed AGNs, the QSO2s, in reproducing the 2–10 keV source counts at relatively bright fluxes. We compare a model where the evolution of absorbed AGNs is faster than that of unabsorbed ones, with a standard model where absorbed and unabsorbed AGNs evolve at the same rate. It is found that an increase by a factor of ~ 2 from $z = 0$ to $z \sim 1.3$ in the ratio between absorbed and unabsorbed AGNs would provide a significant improvement in the data description. Finally, we make predictions on the AGNs to be observed in deep X–ray surveys which contain information on the AGN space density at high redshift.

Key words. X–rays: galaxies – galaxies: nuclei – cosmology: diffuse radiation

1. Introduction

Recent surveys have provided strong evidence that the extragalactic X–ray background (XRB) is mainly due to the integrated emission of single sources. In the soft 0.5–2 keV energy range about 70–80% of the XRB intensity has been resolved by ROSAT at a limiting flux of 10^{-15} erg cm^{-2} s^{-1} (Hasinger et al. 1998). The resolved fraction increases up to $\sim 90\%$ when adding the Chandra results down to a flux of 2.3 10^{-16} erg cm^{-2} s^{-1} (Mushotzky et al. 2000; Giacconi et al. 2000). In the hard 2–10 keV energy range ASCA and BeppoSAX resolved about 25–30% of the XRB (Ueda et al. 1999; Della Ceca et al. 2000; Giommi et al. 2000). When adding Chandra data (Mushotzky et al. 2000; Giacconi et al. 2000) more than 60% of the hard XRB is resolved. Most of the ROSAT and ASCA sources have been optically identified as Active Galactic Nuclei (AGNs; Schmidt et al. 1998; Akiyama et al. 2000, hereafter Ak00). The optical identifications for the Chandra sources are not complete, however AGNs seem to constitute the main population (Barger et al. 2000). These results have confirmed the predictions of AGN synthesis models of the XRB, originally proposed by Setti & Woltjer (1989) and subsequently refined into more detailed variants (e.g. Madau et al. 1994; Comastri et al. 1995); the XRB spectrum is reproduced by summing the contribution of unobscured and obscured AGNs. In these models, the hard spectrum of obscured AGNs is crucial in reproducing the XRB spectral shape above 2 keV.

The existence of a population of luminous absorbed AGNs, the QSO2s, is still a debated issue. Some QSO2s could be hidden in the Ultraluminous IRAS Galaxies (ULIRGs; Kim & Sanders 1998). Indeed, many ULIRGs do show AGN signatures in their spectra (Veilleux et al. 1999). Also, examples of luminous absorbed AGNs could be represented by ROSAT sources with very red colours ($R-K \gtrsim 5$) detected at faint fluxes in the Lockman Hole (Hasinger et al. 1999). Finally, another interesting possibility, which however is still to be verified, is that QSO2s appear as normal blue, broad lined QSOs in the optical. While luminous AGNs with only narrow optical lines are not commonly observed (see e.g. Halpern et al. 1999), ASCA and BeppoSAX have found luminous AGNs with a hard X–ray spectrum showing broad lines in the optical (Ak00; Fiore et al. 2000). If the X–ray hardness is due to cold gas absorption, one could therefore suspect that these objects have different dust–to–gas properties with respect to low luminosity AGNs, where X–ray absorption is generally coupled with an optical type 2 (only narrow lines) classification (Maiolino et al. 2000; Risaliti et al. 2000).

Recent works (Gilli et al. 1999; hereafter Paper I; Pompilio et al. 2000) suggested that the evolution of obscured AGNs might be different from that of unobscured

Send offprint requests to: R. Gilli

ones, with the number ratio R between obscured and unobscured AGNs increasing with redshift. Observational data seem to confirm this suggestion. Indeed, Reeves & Turner (2000) found that in a sample of radio loud and radio quiet QSOs observed by ASCA the fraction of X–ray absorbed AGNs increases with redshift.

The density of high redshift AGNs has been determined in the optical (Schmidt et al. 1995) and in the radio (Shaver et al. 1999) bands. It is found that the AGN density declines above $z \sim 3$, as recently confirmed by results from the Sloan Digital Sky Survey (Fan et al. 2000). In the X–rays the situation is uncertain. The behaviour of the soft X–ray Luminosity Function (XLF) derived by Miyaji et al. (2000a, hereafter Mi00a) from ROSAT data is indeed consistent with a constant AGN density above $z \sim 2$.

In this work we examine XRB synthesis models under different assumptions in the input parameters. We check the differences in reproducing all the available X–ray constraints between a standard model where the ratio R does not evolve with the redshift and a model where absorbed AGNs evolve more rapidly than unabsorbed ones. We analyze the effects of neglecting QSO2s when the XRB intensity is reproduced only with unobscured AGNs and low luminosity absorbed AGNs. Finally, we compare two alternative scenarios where the density of AGNs at high redshift is constant or declines above $z \sim 3$.

Throughout this paper the deceleration parameter and the Hubble constant are given the values $q_0 = 0.5$ and $H_0 = 50$ km s^{-1} Mpc^{-1}.

2. The models

2.1. The spectra

The input AGN spectra have been divided into unabsorbed AGNs and absorbed AGNs with $\log N_{\rm H} = 21.5$, 22.5, 23.5, 24.5, 25.5, as described in Paper I. With respect to Paper I we introduced a change in the soft excess of unabsorbed sources to get a better agreement with observational data. Indeed, the soft excess is not a general property of the spectra of unobscured AGNs. Below $z \sim 0.3$, where a soft excess is observable in the ASCA band, about 50% of QSOs (George et al. 2000; Reeves & Turner 2000) and 20% of the Seyfert 1s (Reynolds 1997) are found to have a soft excess. In the Reeves & Turner (2000) sample the median ratio between the soft excess component and the primary power law in the 0.5–2 keV band is 0.19. We have then approximated this situation by considering a soft excess in *all* the unabsorbed AGNs with a ratio lower by a factor of ~ 2 than the median value of Reeves & Turner (2000). This soft excess is parametrized with a power law with photon index $\Gamma = 2.4$ below 1 keV.

Another difference with respect to Paper I is in the spectrum of AGNs absorbed with $\log N_{\rm H} = 24.5$, where we have now introduced an approximated correction for Compton scattering. We interpolated the AGN spectra of Matt et al. (1999) (see their Fig. 4) deriving a function to correct from the case where only photoelectric absorption is considered. When Compton scattering is added, the intensity of the spectrum of AGNs with $\log N_{\rm H} = 24.5$ decreases by a factor of ~ 2 at 30 keV. We note that the effect of Compton scattering is negligible for the other classes of AGNs in our model with lower absorption. Following Paper I, we have adopted a pure reflection spectrum for sources with $\log N_{\rm H} = 25.5$ since no transmitted component is expected at this absorption level. We remind that a soft component has been considered in the input spectra of absorbed AGNs, parametrized with a power law with $\Gamma = 2.3$, normalized to be 3% of the primary de–absorbed power law at 1 keV.

2.2. The number of obscured AGNs

In our models we fix the local ratio between absorbed and unabsorbed AGNs to $R = 4$. As discussed in Paper I this value is derived by Maiolino & Rieke (1995) as the local ratio between Seyfert 2 and Seyfert 1 galaxies in the optical. Since in the local Universe most of the Seyfert 1 galaxies are unabsorbed in the X–rays (Schartel et al. 1997), $R = 4$ can be used in the X–ray domain as well. We also adopt $R = 4$ for high luminosity AGNs, although this number is uncertain. The distribution of the absorbing column densities is assumed to be that derived by Risaliti et al. (1999), where $\sim 50\%$ of the objects have $\log N_{\rm H} \leq 24$.

We will explore a standard model (model A) where the ratio $R = 4$ does not change with redshift and a model (model B) where the ratio R increases with redshift as follows:

$$R(z) = 4(1+z)^p \qquad z < z_{\rm cut}$$
$$R(z) = R(z_{\rm cut}) = 10 \quad z \geq z_{\rm cut}$$

where $z_{\rm cut}$ is the redshift at which AGNs stop evolving. The absorption distribution is assumed not to vary with redshift and/or luminosity. The ratio R is assumed not to vary with luminosity.

2.3. The XLF

The contribution of unabsorbed and absorbed AGNs to the XRB is evaluated by integrating the XLF of unabsorbed and absorbed objects, respectively. The XLF of absorbed AGNs is completely unknown, while the XLF of unabsorbed AGNs is usually assumed to coincide with the XLF of broad line AGNs. As stated in the previous Section, a mismatch between the optical and the X–ray classification is sometimes observed, therefore considering the XLF of broad line AGNs as the XLF of X–ray unabsorbed AGNs cound not be appropriate. In our model we refer to the XLF derived by Mi00a from a sample of ~ 700 AGNs detected by ROSAT, which includes all those objects that are classified as AGNs, irrespectively of any distinction into type 1 and type 2 subclasses. These authors find that a Luminosity Dependent Density Evolution (LDDE), where the evolution rate drops with decreasing

AGN luminosity, provides a good representation of the data, while a Pure Luminosity Evolution (PLE) or a Pure Density Evolution (PDE) are rejected.

Although derived in the soft band, and then mainly populated by X–ray unabsorbed AGNs, the XLF of Mi00a is expected to include also some absorbed AGNs, which could show up because of their soft components or, for sources at high redshift, because of the K–correction. Also, the Mi00a XLF is given in the observed and not in the rest frame 0.5–2 keV band. We have therefore adopted the following approach to obtain a self–consistent model. First we have considered the LDDE1 representation of Mi00a, where we have arbitrarily modified some parameters to get a rest frame 0.5–2 keV XLF for unabsorbed AGNs only. The rest frame 0.5–2 keV XLFs for the AGNs in each absorption class of our model are then obtained by multiplying the XLF of unabsorbed AGNs by $R \times f_i$, where f_i is the fraction of AGNs in each absorption class according to the distribution of Risaliti et al. (1999). The modified XLF parameters were then tuned to obtain a good fit to the XRB by summing the contribution of unobscured and obscured AGNs.

Once the XRB spectrum has been fitted, we calculate the *observed* XLF for each absorption class in our model, applying the corrections for the absorption and the K–correction. Finally we sum up all the observed XLF for the individual absorption classes to derive the total observed XLF predicted by the model, which can be compared with the binned XLF data quoted by Miyaji et al. (2000b).

3. Results

3.1. The XRB spectrum

The parameters of the LDDE1 description (Mi00a) which we tune in our models are γ_1, L_a and z_{cut}. They represent respectively the slope of the low luminosity part of the XLF, the luminosity below which the density evolution rate starts to drop, and the redshift at which the evolution stops. Their values for models A and B are listed in Table 1. In model B we fixed $R(0) = 4$ and $R(z_{cut}) = 10$, therefore the two models have the same number of free parameters. Following Paper I, the XLF was integrated between $L_{0.5-2} = 10^{41}-10^{49}$ erg s^{-1} and $z = 0-4.6$. Given our assumptions, the XLF of absorbed AGNs in model B evolves according to $(1+z)^{p_{abs}}$, where $p_{abs} = 6.19$. The fit to the XRB spectrum is shown in Fig. 1. The parameters were tuned in order to obtain the same XRB intensity at 5 keV for both models. In the 2–10 keV band the uncertainties in the measured level of the XRB are of the order of 30–40% between different missions (see Vecchi et al. 1999). We chose to fit the XRB intensity of the ASCA data (Miyaji et al. in preparation; Gendreau et al. 1995) which represents a median level among the lowest and highest intensities measured by HEAO–1 (Gruber 1992; Gruber et al. 1999) and BeppoSAX (Vecchi et al. 1999), respectively. As seen in Fig. 1 both models provide a good fit to the XRB spectrum and are identical in the 3–20 keV energy range. As in Paper I, we have also added the contribution of clusters of galaxies, which is non negligible only below ~ 3 keV. Given the higher fraction of absorbed AGNs in model B, the resulting XRB spectrum is harder than that calculated according to model A.

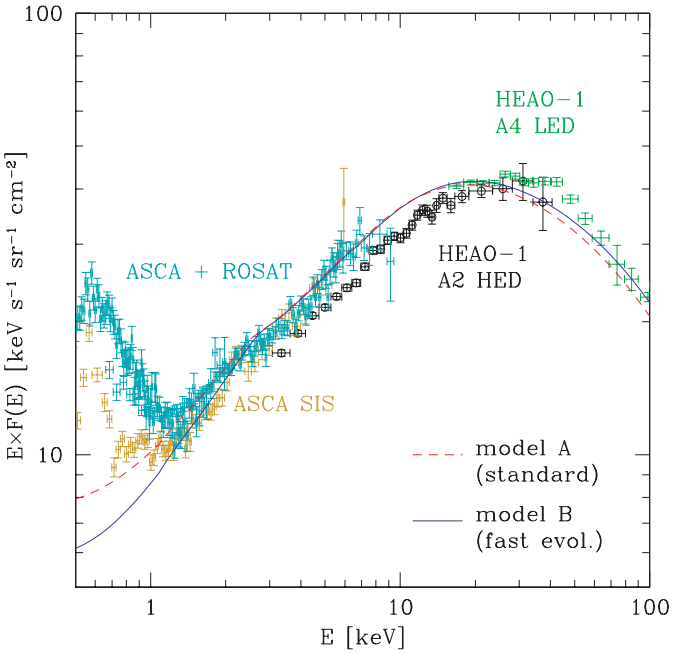

Fig. 1. The fit to the XRB given by model A and model B. The data below ~ 10 keV are from ASCA SIS (Gendreau et al. 1995) and from a combined ASCA GIS + ROSAT PSPC analysis in the ASCA Large Sky Survey region (Miyaji et al. in prep.). The data in the 3–40 keV and 15–100 keV ranges are respectively from the A2 HED and A4 LED detectors on board HEAO–1 (Gruber 1992; Gruber et al. 1999)

Table 1. Model parameters compared with those of Mi00a

Parameter	model A QSO2s	model B QSO2s	model C no QSO2s	Mi00a
γ_1	0.62	0.62	0.62	$0.75^{+0.15}_{+0.15}$
$\log L_a$	44.3	44.65	44.4	44.1^a
z_{cut}	1.54	1.32	1.38	$1.57^{+0.15}_{+0.15}$
$R(0)$	4	4	4^b	
$R(z_{cut})$	4	10	10^b	

Errors in the Mi00a values are at 90% confidence level.
[a]Fixed value by Mi00a.
[b]Ratio at low luminosity. At high luminosity $R(z) = 0$.

3.2. The soft XLF

Starting from the assumed 0.5–2 keV rest frame XLF and after applying corrections for the absorption and the redshift we have reconstructed the *total* AGN XLF in the *observed* 0.5–2 keV band according to the two models, which can be compared with the data of Miyaji et al. (2000b).

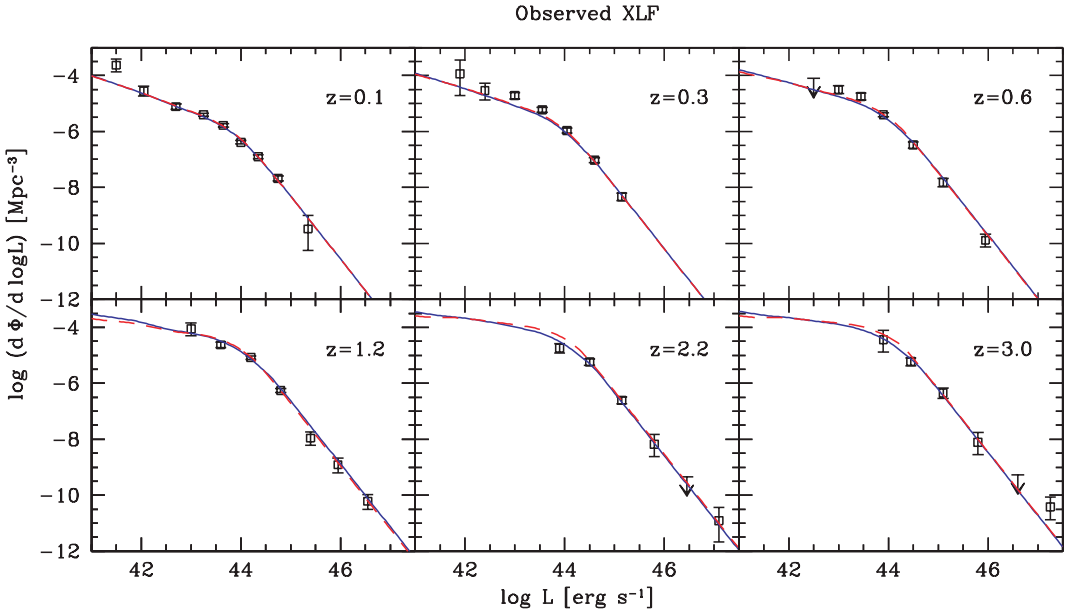

Fig. 2. Comparison between the total observed AGN XLF (Miyaji et al. 2000b) and those predicted by model A (dashed line) and model B (solid line) by summing up the contribution of unabsorbed and absorbed AGNs

In Fig. 2 we show this comparison. Both models provide a good fit to the data. The predictions are almost identical at low redshift, with some differences in the two highest redshift bins. We have performed a χ^2 test to verify the goodness of the fit; the results for the two models are shown in Table 2.

3.3. The X–ray source counts

We have then compared the predictions of the competing models with the source counts observed in the 0.5–2 keV and 2–10 keV energy bands. In our calculation we have considered the fact that the observed log$N$–log$S$ are derived from samples of objects limited in count–rate rather than in flux. Since X–ray instruments have higher sensitivity at low energies, soft sources can be detected at fainter fluxes with respect to hard sources. When converting from count rates to fluxes a single conversion factor is usually assumed in published works (corresponding to an average spectrum). This implies that the flux of a source harder or softer than the average one is underestimated or overestimated, respectively. Therefore, since the number density of sources increases with decreasing flux, at any measured flux in the log$N$–log$S$ the ratio between absorbed and unabsorbed AGNs is underestimated. To cope with this situation we have therefore introduced into our log$N$–log$S$ calculations the same instrumental bias. Correction for the ROSAT PSPC and ASCA SIS0 effective areas have been considered in the 0.5–2 keV and 2–10 keV band, respectively. The ROSAT PSPC correction has been also adopted when calculating the predicted XLF shown in Fig. 2. The inclusion of the instrumental effects is discussed in detail in the Appendix.

The comparisons of the model predictions with the soft and the hard counts are shown in Figs. 3 and 4, respectively.

We performed a χ^2 test on the soft counts to evaluate statistically the differences between model A and B. Since the datapoints of Mi00a are not independent, we have considered literature data derived from different ROSAT surveys in addition to the Chandra data. The survey areas adopted to calculate the AGN densities have been corrected for incompleteness in the optical identifications. All the ROSAT AGN densities used in the χ^2 test and shown in Fig. 3 are in agreement within 1σ with those of Fig. 6 of Mi00a apart for the one at 3 10^{-14} erg cm^{-2} s^{-1} derived from the RIXOS survey (Page et al. 1996; Mason et al. 2000), which is lower by 30% (4σ). Since at the faint Chandra fluxes the optical identifications are scarce, we compare the models with the total number of X–ray sources. The results of the χ^2 test are shown in Table 2.

Model B provides a better agreement also with the hard data with respect to model A, despite of discrepancies in the density of hard sources of the order of 20% between ASCA and BeppoSAX data and 40% between Chandra results from different surveys. The curves plotted in Fig. 4 include also the contribution of clusters of galaxies (which is negligible below $\sim 10^{-14}$ erg cm^{-2} s^{-1}). At high fluxes the AGN density predicted by the model is in agreement with that measured by Piccinotti et al. (1982)[1].

We performed a χ^2 test over a series of total hard counts derived from separate surveys (shown in Fig. 4)

[1] In Fig. 4 we plot the total source counts also for the Piccinotti sample, contrary to Paper I where we plotted only the AGN counts.

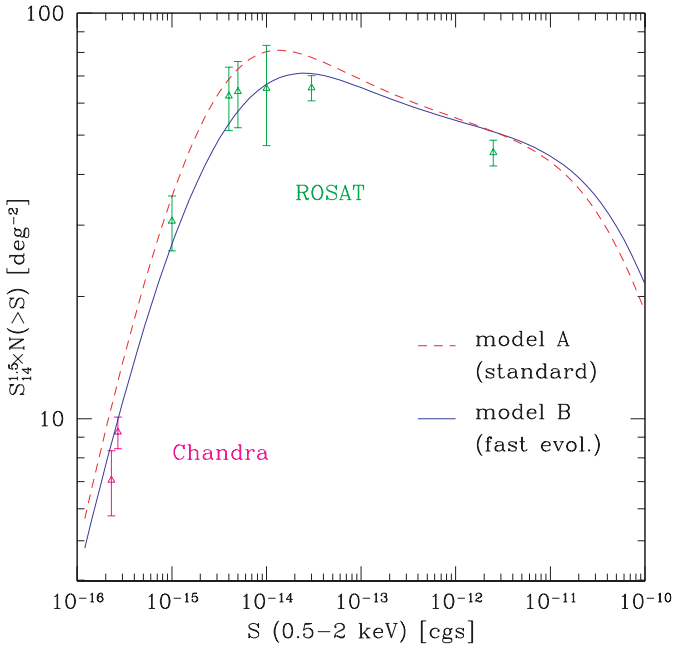

Fig. 3. The predictions of model A and B compared with the 0.5–2 keV source counts. In this and in the following figures, source counts are plotted as $S_{14}^{1.5} \times N(>S)$, where S_{14} is the flux in units of 10^{-14} erg s^{-1} cm^{-2}, and errorbars refer to 1σ uncertainties. With decreasing flux, the data are derived from Mi00a, Mason et al. (2000), Bower et al. (1996), Mi00a, Zamorani et al. (1999), Hasinger et al. (1998), Giacconi et al. (2000), and Mushotzky et al. (2000). The 5 points at higher fluxes contain only AGNs, the remaining three points at lower fluxes are total counts

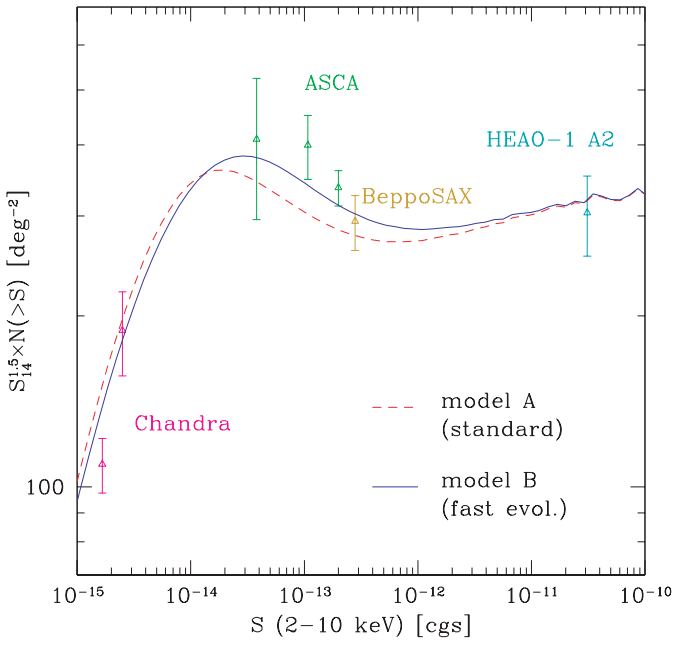

Fig. 4. The predictions of model A and B (considering AGNs plus clusters of galaxies) compared with the 2–10 keV total counts. With decreasing flux, the data are from Piccinotti et al. (1982), Giommi et al. (2000), Ueda et al. (1999), Cagnoni et al. (1998), Ogasaka et al. (1998), Mushotzky et al. (2000), and Giacconi et al. (2000)

Table 2. χ^2 test on the XLF and source counts

Data set	χ^2/dof	
	model A	model B
0.5–2 keV XLF	54.4/38	49.0/38
0.5–2 keV counts	34.3/8	8.3/8
2–10 keV counts	20.5/7	8.5/7

and then independent from each other. The results are shown in Table 2.

We have verified that the two models are in agreement with the $N_{\rm H}$ distribution observed in the Piccinotti sample (Schartel et al. 1997). Since $R(0) = 4$ for both models and since the Piccinotti sample is dominated by local AGNs, the $N_{\rm H}$ distributions predicted by the two models are identical.

3.4. Redshift distributions

The models have been also checked against the redshift distribution of AGNs in flux limited samples. We first consider the data from the ROSAT Ultradeep HRI Survey in the Lockman Hole (Hasinger et al. 1999; Lehmann et al. 2001). With an exposure of 1 Msec the achieved 0.5–2 keV limiting flux is 1.2 10^{-15} erg s^{-1} cm^{-2}. We consider only the subsample of sources with an offset angle from the aimpoint below 12 arcmin, in order to avoid vignetting effects and then non uniform limiting fluxes across the field. The optical identifications of this sample are almost complete and 50 AGNs have been identified: 40 of them have broad lines (ID classes *a, b, c* according to the classification scheme of Schmidt et al. 1998), while 10 have no broad lines (ID classes *d, e*). Four AGNs without broad lines have only a photometric redshift estimate, which, if proven to be correct, would place them at $z > 1$.

When comparing the model with the data, corrections for the HRI effective area have been introduced into the calculations. Since the HRI sources have been detected by using the full HRI band 0.1–2.4 keV, when converting from the count rate to a 0.5–2 keV flux, the conversion factor varies by $\pm 40\%$ for photon indices $\Gamma = 2.0 \pm 0.7$. This introduces a strong bias against hard (absorbed) sources which is introduced in our computations (see details in the Appendix). Besides the redshift distribution for total AGNs we calculated the distributions for the AGNs with $\log N_{\rm H} < 22$ and $\log N_{\rm H} > 22$ separately, which have been compared with those of AGNs with ID classes *a, b, c* and *d, e*, respectively (Fig. 5). Given the possible mismatch between optical and X–ray classification mentioned in Sect. 1, this comparison might not be strictly appropriate. However, we consider this as a first order check to the model. The ratio between AGNs with $\log N_{\rm H} < 22$ and $\log N_{\rm H} > 22$ predicted by model A and B is 42/8 and 36/14 respectively, to be compared with the ratio 40/10 between AGNs in the *a, b, c* classes and AGNs in the *d, e* classes (the total number of AGNs is normalized to the observed

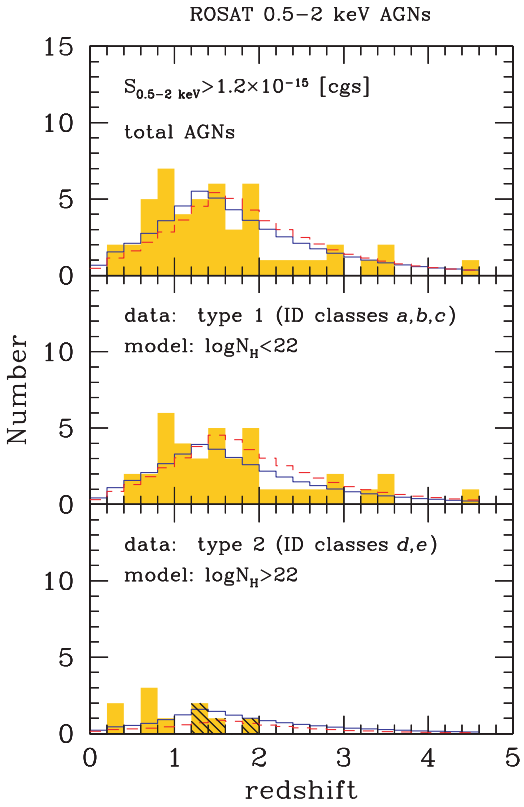

Fig. 5. The redshift distribution predicted by model A (dashed) and B (solid) compared with the AGN sample from the ROSAT Ultradeep HRI Survey (Hasinger et al. 1999). The shaded histogram refers to AGNs having only a photometric redshift estimate

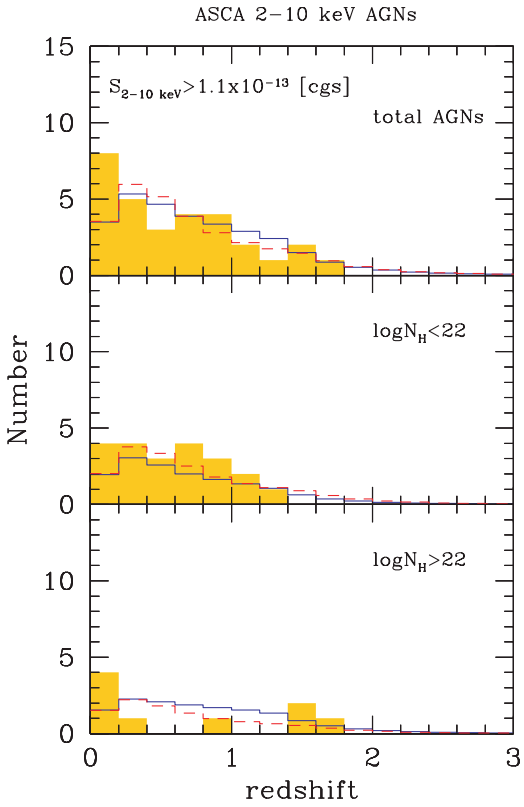

Fig. 6. The redshift distribution predicted by model A (dashed) and B (solid) compared with the AGN sample from the ASCA Large Sky Survey (Ak00). Four blue, broad lined QSOs at $z > 0.8$ with hard X–ray spectra have been included among the AGNs with $\log N_{\rm H} > 22$

Table 3. Kolmogorov–Smirnov test on the redshift distributions

Data set	$P_{\rm KS}$	
	model A	model B
ROSAT total	0.02	0.23
$\log N_{\rm H} < 22$	0.26	0.90
$\log N_{\rm H} > 22$	0.01	0.03
ASCA total	0.43	0.23
$\log N_{\rm H} < 22$	0.35	0.33
$\log N_{\rm H} > 22$	0.35	0.24

one). We have also calculated the probability that the observed sample has been drawn from the predicted distribution according to a Kolmogorov–Smirnov (KS) test. The calculated probabilities are quoted in Table 3. Model B is slightly favored by the test.

Then we compared the predictions of the models with the redshift distributions of AGNs in the 2–10 keV band. We consider the hard sample detected by the SIS instrument in the ASCA Large Sky Survey (Ueda et al. 1999) at a limiting flux of 10^{-13} erg cm^{-2} s^{-1} between 2–10 keV, which has been completely identified by Ak00. They find 30 AGNs in a sample of 34 objects (plus 2 clusters of galaxies, 1 star and 1 unidentified source). These authors also estimate a column density for the AGNs from a hardness ratio analysis, assuming an intrinsic spectral index $\Gamma = 1.7$. The ratio between AGNs with $\log N_{\rm H} < 22$ and $\log N_{\rm H} > 22$ is found to be 21/9. On the basis of their hardness ratios also 4 normal, blue and broad lined QSOs with $z > 0.8$ are considered to have $\log N_{\rm H} > 22$. The unidentified source has a very hard X–ray spectrum ($\Gamma < 1$) and is presumably an obscured AGN. The predicted ratio $N(\log N_{\rm H} < 22)/N(\log N_{\rm H} > 22)$ is 19/11 and 15/15 for model A and B, respectively (the total number of AGNs is normalized to the observed one). The comparison between the observed and predicted redshift distributions for the Ak00 sample is shown in Fig. 6. The probability that the sample is drawn from the calculated distributions is evaluated with a KS test and quoted in Table 3. Here the two models perform equally well.

3.5. QSO2s

We checked the role of high luminosity absorbed AGNs, the QSO2s, by fitting the XRB only with unabsorbed AGNs (at all luminosities) and low luminosity absorbed AGNs. Following Paper I we introduced an exponential cut off in the 0.5–2 keV XLF of absorbed objects, where $L_{\rm s} = 2\ 10^{44}$ erg s^{-1} is the intrinsic e–folding luminosity. The ratio between absorbed and unabsorbed

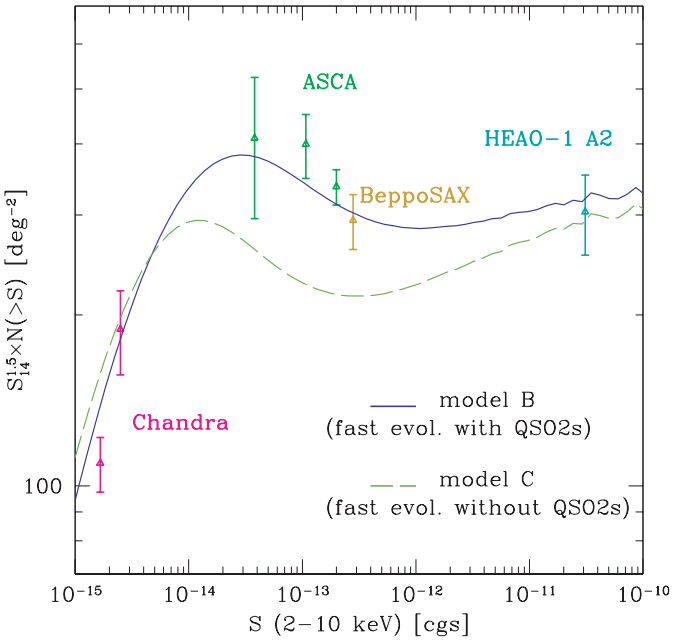

Fig. 7. The predictions of model B and C (considering AGNs plus clusters of galaxies) compared with the 2–10 keV total counts. Datapoints are the same as in Fig. 4

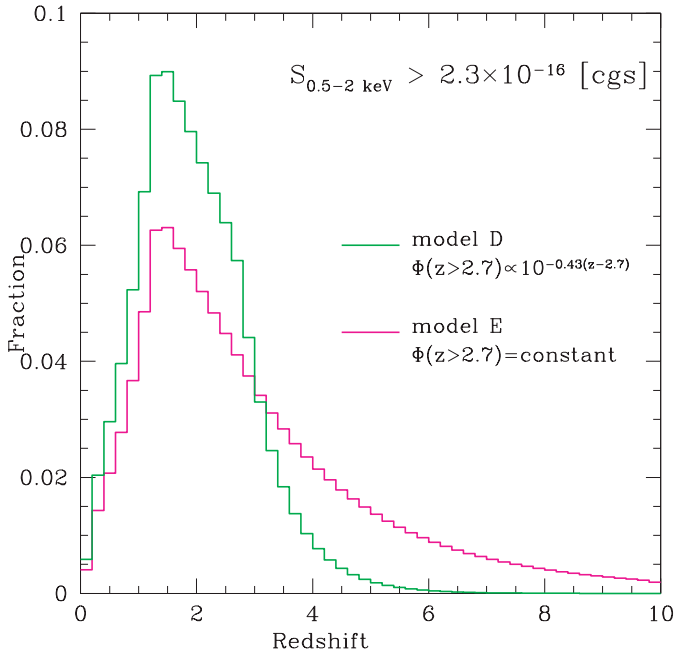

Fig. 8. Redshift distribution for the Mushotzky et al. (2000) 0.5–2 keV sample as expected from model D and model E. The same distribution is also expected for the Giacconi et al. (2000) 0.5–2 keV sample

AGNs in the low luminosity regime is assumed to increase from $R(0) = 4$ to $R(z_{\rm cut}) = 10$ as in model B. Then we tuned the parameters of the XLF in order to reproduce the XRB spectrum (model C). The fit to the XRB spectrum is as good as in model B, while a major difference is seen in the hard counts (Fig. 7). When trying to reproduce the XRB without QSO2s, the 2–10 keV counts at relatively bright fluxes are severely underestimated (with a significance higher than 4.5σ at 2 10^{-13} erg cm^{-2} s^{-1}), since in this case the hard XRB is mainly due to low luminosity objects showing up at faint fluxes.

3.6. High–redshift AGNs in X–ray surveys

Deep surveys should allow to determine the behaviour of the AGN XLF at high redshift. From optical and radio surveys a decline above $z \sim 3$ is observed, while from X–ray surveys a constant density above $z \sim 2$ is not ruled out (see Fig. 11 in Mi00a). In the previous calculations we assumed that the density of AGNs is constant in the range from $z = z_{\rm cut}$ to $z = 4.6$ and then it suddenly drops to zero. Now, starting from model B, we consider the following scenarios. In the first case (model D) we assume that the AGN density above $z = 2.7$ decreases by a factor 2.7 per unit redshift as found for optical QSOs by Schmidt et al. (1995; see also Fan et al. 2000). In the second case (model E) we assume that the AGN density is constant up to $z = 10$. Model D provides a better description of the overall X–ray constraints (hard XRB spectrum, soft and hard counts, soft and hard redshift distributions) than model E. In particular the Chandra data are better accounted for in model D, since high redshift (low fluxes) AGNs are removed from the model. The real behaviour of the AGN density at high redshift will be proven when complete optical identification of deep surveys will be available. We calculated the redshift distribution predicted by model D and E at $S = 2.3\ 10^{-16}$ erg cm^{-2} s^{-1}, the limiting flux of the 0.5–2 keV sample in Mushotzky et al. (2000), which is also very close to the limiting flux of the 0.5–2 keV sample in Giacconi et al. (2000). The results are shown in Fig. 8. The percentage of AGNs above $z = 5$ expected from model D and E are significantly different: 0.7% and 15%, respectively. The total AGN density at $z > 5$ is 16 deg^{-2} for model D and 500 deg^{-2} for model E. The Haiman & Loeb (1999) model predicts about 500 deg^{-2} AGNs at $z > 5$ for the same band and limiting flux.

4. Discussion

In this work some changes have been made in the model assumptions with respect to Paper I. The weakening of the soft excess component slightly hardens the XRB spectrum and increases the 2–10 keV counts by less than 10%. In general, our results are not significantly affected by the precise parametrization of the soft excess. The Compton scattering correction in the spectra of absorbed AGNs with $\log N_{\rm H} = 24.5$ reduces by 10–15% the intensity of the XRB at 30 keV. The corrections for the instrumental effects (see the Appendix) are relevant on the expected ratio between absorbed and unabsorbed AGNs in different surveys, but do not affect the expected total surface density of AGNs. The major change, instead, concerns high luminosity obscured AGNs, the QSO2s, which are now assumed to constitute a large population of sources.

As already recognized by Comastri (2000) and as shown in Fig. 7, QSO2s are fundamental in reproducing the ASCA counts. In model C we arbitrarily assume $L_{\rm s} = 2\ 10^{44}$ erg s^{-1} as the intrinsic e–folding luminosity in the 0.5–2 keV XLF of absorbed AGNs. Objects with this luminosity could still be considered in the Seyfert luminosity domain. If we very conservatively assume $L_{\rm s} = 10^{45}$ erg s^{-1}, corresponding to a bolometric luminosity higher than 10^{46} erg s^{-1} (Elvis et al. 1994), the 2–10 keV counts at $2\ 10^{-13}$ erg cm^{-2} s^{-1} are still underestimated with a significance higher than 3σ. As shown in Figs. 5 and 6, the existence and the assumed abundance of QSO2s are consistent with the AGN redshift distributions observed in ROSAT and ASCA surveys.

The nature and the number of obscured QSOs is still debated. In Paper I, under the assumption that the absorbed X–ray photons are re–emitted as infrared photons, we estimated that, if every ultraluminous infrared galaxy is powered by an AGN and is therefore considered as a QSO2, the ratio QSO2s/QSOs in the local Universe is at most 2. This upper limit could be relaxed if a fraction of the X–ray absorbed objects have normal blue and broad lined spectrum in the optical (Reeves & Turner 2000; Ak00; Fiore et al. 2000). Radio Loud QSOs were already found to be X–ray absorbed, and the X–ray weakness of Broad Absorption Lines QSOs has also been interpreted as due to X–ray absorption (Brandt et al. 2000). Furthermore, a large population of X–ray absorbed, broad lined QSOs with a red continuum seems to emerge from the analysis of grism based surveys (Risaliti et al. 2000) which would join the population of radio selected red QSOs discovered by Webster et al. (1995). However, given the uncertainties affecting the X–ray spectra of these sources, XMM observations are necessary to confirm the existence of a population of broad lined, X–ray absorbed QSOs.

On the other hand, examples of QSOs obscured both in the optical band and in the X–rays could be represented by a few ROSAT sources in the Lockman Hole with very red colours ($R-K \gtrsim 5$, Hasinger et al. 1999). This might suggest that the central AGN is heavily obscured and we are observing the colours of the host galaxy. As shown by Hasinger (2000), one of these sources, which has been observed from radio to X-rays, shows a spectral energy distribution remarkably similar to that of the luminous absorbed AGN NGC 6240 (Vignati et al. 1999).

Overall the number of QSO2s is not yet established, for simplicity we fixed the local ratio between absorbed and unabsorbed QSOs to 4 as in the case of lower luminosity AGNs.

As it is apparent from Table 2, a model where the evolution of absorbed AGNs is faster than that of unabsorbed ones provides a better representation of the main X–ray observational constraints. By summing the χ^2 of the 0.5–2 keV XLF, 0.5–2 keV log$N$–log$S$ and 2–10 keV log$N$–log$S$, the improvement of model B with respect to model A is significant at $> 99.99\%$ confidence level ($\Delta\chi^2 = 43.4$). Now we discuss some uncertainties which could affect the significance of this result. A first problem could be represented by the XRB normalization. Since there are variations of about 40% in the 2–10 keV XRB intensity measurements (see e.g. Vecchi et al. 1999), fitting different XRB intensities would lead to different predictions for the number counts in the soft and hard band. We fitted the XRB intensity measured by ASCA, which represents a median level between the highest measurement performed by BeppoSAX (Vecchi et al. 1999) and the lowest one performed by HEAO–1 A2 (Gruber 1992; Gruber et al. 1999). We note that the data from the A2 HED experiment on board HEAO–1 seem to be lower by $\sim 10\%$ not only with respect to the ASCA XRB data, but also with respect to the high energy data measured by the A4 LED experiment (see Fig. 2 in Gruber et al. 1999). Thus, a miscalibration of $\sim 10\%$ of the A2 HED data could account for the some of the systematic differences of intensity in the XRB measurements.

In fitting the 2–10 keV XRB intensity measured by HEAO–1 A2 by changing the free parameters of the models (see Table 1) the AGN counts predicted in the soft and hard band would both be reduced by 20–30% at the Chandra fluxes, while the decrement is negligible above $\sim 10^{-13}$ erg cm^{-2} s^{-1} and $\sim 5\ 10^{-12}$ erg cm^{-2} s^{-1}, respectively. Even in this case the fast evolution model would provide a better agreement with the data. Also in the case of a fit to the XRB intensity measured by BeppoSAX model B provides a better description of the data when compared to model A.

A second problem could arise from the choices made in the χ^2 tests performed on the log$N$–log$S$. When dealing with the 0.5–2 keV log$N$–log$S$ we have compared the AGN densities predicted by the models with those measured by ROSAT. Since for the Chandra data the optical identifications are sparse, we compared the predictions of the model with the total number of sources. We note that in our models the cluster contribution at the Chandra fluxes is negligible. However, if other classes of sources are contributing to the Chandra counts and the AGNs counts are significantly lower than the total ones, model B would always provide a better representation of the data.

When considering the 2–10 keV log$N$–log$S$ we compared the data with the total density of objects (AGN plus clusters of galaxies) predicted by the models, since optical identifications are incomplete for most of the adopted datasets. We note however that our models are in agreement with the separate measurements of the AGN and cluster densities determined by Piccinotti et al. (1982) and Ak00. We consider it appropriate to compare the total source density measured by the different surveys in the 2–10 keV band with the AGN + cluster model predictions, since >95% of the sources in the Ak00 sample are AGNs or clusters. We note that without the correction for the ASCA instrumental response the ratio $N(\log N_{\rm H} < 22)/N(\log N_{\rm H} > 22)$ predicted by model B for the Ak00 sample would have been 12/18 rather than 15/15. As pointed out by Comastri (2000), in previous synthesis models the number of unabsorbed AGNs

predicted at the ASCA fluxes seemed to be in disagreement with that observed. When considering instrumental effects much of the discrepancy can thus be explained.

After the discovery of hard X–ray spectra in a small sample of nearby elliptical galaxies (Allen et al. 2000) it was proposed by Di Matteo & Allen (1999) that a substantial fraction of the XRB intensity could arise from advection dominated flows in elliptical galaxies. However, in this case elliptical galaxies with normal optical spectra should represent a significant fraction of the 2–10 keV ASCA counts, at variance with the findings of Ak00.

Our models are found to be in good agreement with the AGN redshift distributions in the soft and hard bands, as checked with the Kolmogorov–Smirnov tests. Also, they are in agreement with the relative fraction of absorbed AGNs found in flux limited samples. A possible discrepancy could be recognized in the ratio between AGNs with $\log N_{\rm H} < 22$ and $\log N_{\rm H} > 22$ observed in the Ak00 sample and that predicted by model B. However, this is only a 1σ effect. Also, the column density estimated by Ak00 from the hardness ratio analysis assuming a simple absorbed power law model could have been underestimated if a soft component is commonly present in the spectra of absorbed AGNs, as assumed in our models. This is likely to be the case, as shown by the X–ray color–color diagrams for ASCA and BeppoSAX sources (Della Ceca et al. 1999; Fiore et al. 2000).

Our models slightly overpredict the Chandra source counts in the soft band, and probably also in the hard band (referring to the data of Giacconi et al. 2000). Introducing a cut off at $z = 2.7$ in the AGN density as observed in the optical surveys would provide a better description of the Chandra data, since high redshift AGNs which would show up at faint fluxes would be removed.

The improvement introduced by model B with respect to model A resides essentially in the higher fraction of hard sources and in the lower value of $z_{\rm cut}$. In order to avoid introducing other free parameters we assumed that the value of $z_{\rm cut}$ is the same for absorbed and unabsorbed AGNs. However, we note that a still better fit to the X–ray constraints could be obtained if a lower $z_{\rm cut}$ for absorbed AGNs were used. Indeed, this would imply that a higher fraction of the hard XRB is produced at small redshift, with an increase of the hard counts at the ASCA fluxes and a decrease at the Chandra fluxes. Also, the XRB bump at ~ 30 keV would be better reproduced since the AGN spectral peak at 30–40 keV would be on the average less redshifted. Another improvement is expected in the redshift distributions.

We note that the $N_{\rm H}$ distribution adopted in our models, derived by Risaliti et al. (1999) for a local sample of AGNs, is very similar[2] to that used by Comastri et al. (1995) *to fit* the XRB spectrum, which is mostly produced by objects at higher redshift. It thus seems that it would be difficult to obtain good XRB fits with $N_{\rm H}$ distributions which are very different from the adopted one. Furthermore, this argument suggests that a fast evolution of absorbed sources would be hardly superseded in improving the description of X–ray data by simply changing the $N_{\rm H}$ distribution with redshift.

The significance of a faster evolution of absorbed AGNs might be reduced by systematic uncertainties in the adopted data and further checks with the data from on going deep surveys are needed. If the higher fraction of absorbed AGNs at high redshift is proven to be real, one could try to link this finding to the star formation history in the Universe. A higher merging rate at high redshift could trigger the star formation and the gas flow towards the galaxy centers. As suggested by Fabian et al. (1998), circumnuclear starbursts could obscure most of the nuclear radiation. In this scheme, the higher fraction of obscured sources at high redshift could be explained. This can also be related with the finding that non–axisymmetric morphologies increase the obscuration in AGNs (Maiolino et al. 1999), and that distorted, non–axisymmetric morphologies are more common among galaxies at high redshift.

5. Conclusions

We have presented different synthesis models for the XRB, checking the model predictions with all the available X–ray constraints posed by the source counts, XLF, redshift distributions and absorption distributions. Models assuming a population of high luminosity obscured AGNs, the QSO2s, are found to be consistent with all the available data. Furthermore, the existence of QSO2s is found to be necessary in reproducing the 2–10 keV source counts at relatively bright fluxes ($\sim 10^{-13}$ erg cm^{-2} s^{-1}). We found that a model (model B) where the evolution of absorbed AGNs is faster than that of unabsorbed ones provides a better description of the data with respect to a standard model (model A) where absorbed and unabsorbed AGNs evolve with the same rate. Our models are also in agreement with the first results from Chandra deep surveys. Chandra sources, together with those detected in XMM deep surveys, will provide additional information on the QSO2 population and will verify if the faster evolution of absorbed AGNs is real. Furthermore, the behaviour of the AGN space density at high redshift will be determined when optical identification programs will be completed.

Acknowledgements. We are grateful to T. Miyaji for providing data on the XRB spectrum and AGN XLF, and to P. Tozzi for providing data on the Chandra counts. RG thanks A. Comastri and G. Risaliti for useful discussions. We thank the referee for prompt and constructive comments. This work was partly supported by the Italian Space Agency (ASI) under grant ARS–98–116/22 and by the Italian Ministry for University and Research (MURST) under grant Cofin98–02–32.

[2] Basically the two distributions differ only about the number of AGNs with $\log N_{\rm H} > 25$ (see Fig. 1 of Paper I), which however do not contribute significantly to the XRB intensity.

Appendix A: Corrections for instrumental effects

To allow a consistent comparison between the log$N$–log$S$ and redshift distributions predicted by the models and the literature data, we have taken into account the bias against absorbed sources introduced by the effective area of the X–ray instruments. We describe the procedure adopted when comparing the model predictions with the 0.5–2 keV AGN log$N$–log$S$, which is mainly derived from ROSAT PSPC data. This procedure is analogous to that adopted when considering data from other X–ray instruments. For each absorption class considered in the models we have produced with the XSPEC package a spectrum identical to that considered in the model. The obtained spectra have been folded with the ROSAT PSPC spectral response. We adopted the calibration file `pspcb_gain2_256.rsp` retrieved from the archive in the `ftp://legacy.gsfc.nasa.gov/` website. The file contains the spectral response of the PSPC detector multiplied by the X–ray telescope effective area. We therefore obtained a count rate to flux conversion factor CF_i for each of the AGN spectra assumed in our model. The spectra have also been redshifted and the conversion factors calculated as a function of redshift. When deriving the AGN 0.5–2 keV XLF and counts Mi00a assumed a power law with $\Gamma = 2$ (absorbed by a Galactic column density) to convert from the 0.5–2 keV PSPC count rate to the 0.5–2 keV flux, corresponding to a conversion factor $\mathrm{CF}_* = 0.836$ cts s^{-1}/ (10^{-11} erg cm^{-2} s^{-1}) (see Table 2 in Hasinger et al. 1998). The conversion factor CF_* was used for all the sources, irrespectively of their real spectrum. However, sources with a spectrum harder than $\Gamma = 2$ would produce less photons on the detector at a given flux, therefore a conversion factor lower than CF_* should be used. Analogously, for those sources softer than $\Gamma = 2$ a conversion factor greater that CF_* should be used. Then, a source with a measured flux S would have a real flux $S \times (\mathrm{CF}_*/\mathrm{CF})$, where CF is the conversion factor which would be appropriate for the source spectrum. Therefore, in our calculations of the log$N$–log$S$, at a given flux S we summed the contribution of each absorption class of the model calculated at $S \times (\mathrm{CF}_*/\mathrm{CF}_i)$.

The same procedure has been adopted for the 2–10 keV log$N$–log$S$ and redshift distribution at $S = 10^{-13}$ erg cm^{-2} s^{-1}, which have been corrected for the ASCA SIS0 plus X–ray mirror effective area (calibration file `s0c1g0234p40e1_512_1av0_8i.rsp`). For the 2–10 keV band we adopted $\mathrm{CF}_* = 1.089$ cts s^{-1}/ (10^{-10} erg cm^{-2} s^{-1}), corresponding to $\Gamma = 1.7$. Indeed, a conversion spectrum with $\Gamma = 1.6 - 1.7$ is commonly adopted in the hard X–ray surveys (e.g. Ak00; Cagnoni et al. 1998).

For the redshift distribution of the 0.5–2 keV AGNs calculated at $S = 1.2\ 10^{-15}$ erg cm^{-2} s^{-1} we have considered the corrections for the HRI spectral response and X–ray mirror effective area contained in `hri_90dec01.rsp`. We adopted $\mathrm{CF}_* = 0.586$ cts s^{-1}/ (10^{-11} erg cm^{-2} s^{-1}), which is the conversion factor from the 0.1–2.4 keV HRI cont rate to the 0.5–2 keV flux appropriate for a spectral power law with $\Gamma = 2$.

References

Akiyama, M., Ohta, K., Yamada, T., et al. 2000, ApJ, 532, 700 (Ak00)

Allen, S. W., Di Matteo, T., & Fabian, A. C. 2000, MNRAS, 311, 493

Barger, A. J., Cowie, L. L., Mushotzky, R. F., & Richards, E. A. 2000, AJ, in press [astro-ph/0007175]

Bower, R. G., Hasinger, G., Castander, F. J., et al. 1996, MNRAS, 281, 59

Brandt, W. N., Laor, A., & Wills, B. J. 2000, ApJ, 528, 637

Cagnoni, I., Della Ceca, R., & Maccacaro, T. 1998, ApJ, 493, 54

Comastri, A., Setti, G., Zamorani, G., & Hasinger, G. 1995, A&A, 296, 1

Comastri, A. 2000, Astroph. Lett. and Comm., in press [astro-ph/0003437]

Della Ceca, R., Castelli, G., Braito, V., Cagnoni, I., & Maccacaro, T. 1999, ApJ, 524, 674

Della Ceca, R., Braito, V., Cagnoni, I., & Maccacaro, T. 2000, Mem. SAIt, in press [astro-ph/0007430]

Di Matteo, T., & Allen, S. W. 1999, ApJ, 527, L21

Elvis, M., Wilkes, B. J., Mc Dowell, C., et al. 1994, ApJS, 95, 1

Fabian, A. C., Barcons, X., Almaini, O., & Iwasawa, K. 1998, MNRAS, 297, L11

Fan, X., Strauss, M. A., Schneider, D. P., et al. 2000, AJ, in press [astro-ph/0008123]

Fiore, F., Giommi, P., Vignali, C., et al. 2000, MNRAS, submitted

Gendreau, K. C., Mushotzky, R. F., Fabian, A. C., et al. 1995, PASJ, 47, L5

George, I. M., Turner, T. J., Yaqoob, T., et al. 2000, ApJ, 531, 52

Giacconi, R., Rosati, P., Tozzi, P., et al. 2000, ApJ, submitted [astro-ph/0007240]

Gilli, R., Risaliti, G., & Salvati, M. 1999, A&A, 347, 424

Giommi, P., Perri, M., & Fiore, F. 2000, A&A, in press [astro-ph/0006333]

Gruber, D. E. 1992, in The Proceedings of: The X–ray background, ed. X. Barcons, & A. C. Fabian (Cambridge Univ. Press, Cambridge), 44

Gruber, D. E., Matteson, J. L., Peterson, L. E., & Jung, G. V. 1999, ApJ, 520, 124

Haiman, Z., & Loeb, A. 1999, ApJ, 521, L9

Halpern, J. P., Turner, T. J., & George, I. M. 1999, MNRAS, 307, L47

Hasinger, G., Burg, R., Giacconi, R., et al. 1998, A&A, 329, 482

Hasinger, G., Lehmann, I., Giacconi, R., et al. 1999, in Highlights in X–ray Astronomy in Honor of Joachim Trümper's 65th Birthday. MPE Report, MPE, Garching, in press [astro-ph/9901103]

Hasinger, G. 2000, in The Proceedings of: ISO Surveys of a Dusty Universe, ed. D. Lemke, M. Stickel, & K. Wilke (Springer), in press [astro-ph/0001360]

Kim, D.-C., & Sanders, D. B. 1998, ApJS, 119, 41

Lehmann, I., Hasinger, G., Schmidt, M., et al. 2001, A&A, submitted

Madau, P., Ghisellini, G., & Fabian, A. C. 1994, MNRAS, 270, L17

Maiolino, R., & Rieke, G. H. 1995, ApJ, 454, 95
Maiolino, R., Risaliti, G., & Salvati, M. 1999, A&A, 341, L35
Maiolino, R., Marconi, A., Salvati, M., et al. 2000, A&A, in press [astro-ph/0010009]
Mason, K. O., Carrera, F. J., Hasinger, G., et al. 2000, MNRAS, 311, 456
Matt, G., Pompilio, F., & La Franca, F. 1999, New Astron., 4, 191
Miyaji, T., Hasinger, G., & Schmidt, M. 2000a, A&A, 353, 25 (Mi00a)
Miyaji, T., Hasinger, G., & Schmidt, M. 2000b, A&A, submitted
Mushotzky, R. F., Cowie, L. L., Barger, A. J., & Arnaud, K. A., 2000, Nature, 404, 459
Ogasaka, Y., Kii, T., Ueda, Y., et al. 1998, Astron. Nacht., 319, 47
Page, M. J., Carrera, F. J., & Hasinger, G. 1996, MNRAS, 281, 579
Piccinotti, G., Mushotzky, R. F., Boldt, E. A., et al., 1982, ApJ, 253, 485
Pompilio, F., La Franca, F., & Matt, G. 2000, A&A, 353, 440
Reeves, J. N., & Turner, M. J. L. 2000, MNRAS, 316, 234
Reynolds, C. S. 1997, MNRAS, 286, 513
Risaliti, G., Maiolino, R., & Salvati, M. 1999, ApJ, 522, 157
Risaliti, G., Marconi, A., Maiolino, R., Salvati, M., & Severgnini, P. 2000, A&A, submitted
Schartel, N., Schmidt, M., Fink, H. H., Hasinger, G., & Trümper, J. 1997, A&A, 320, 696
Schmidt, M., Schneider, D. P., & Gunn, J. E. 1995, AJ, 110, 68
Schmidt, M., Hasinger, G., Gunn, J., et al., 1998, A&A, 329, 495
Setti, G., & Woltjer, L. 1989, A&A, 224, L21
Shaver, P. A., Hook, I. M., Jackson, C. A., et al. 1999, in Highly Redshifted Radio Lines, ed. C. Carilli, S. Radford, K. Menten, & G. Langston, ASP Conf. Ser., 156, 163 [astro-ph/9801211]
Ueda, Y., Takahashi, T., Inoue, H., et al. 1999, ApJ, 518, 656
Vecchi, A., Molendi, S., Guainazzi, M., Fiore, F., & Parmar, A. N. 1999, A&A, 349, L73
Vignati, P., Molendi, S., Matt, G., et al. 1999, A&A, 349, L57
Veilleux, S., Kim, D.-C., & Sanders, D. B. 1999, ApJ, 522, 113
Webster, R. L., Francis, P. J., Peterson, B. A., et al. 1995, Nature, 375, 469
Zamorani, G., Mignoli, M., Hasinger, G., et al. 1999, A&A, 346, 731